The International Journal of Advanced Manufacturing Technology (2018) 96:3679–3690
https://doi.org/10.1007/s00170-018-1676-8

ORIGINAL ARTICLE

A decision support system for the validation of metal powder bed-based additive manufacturing applications

Niklas Kretzschmar[1] · Iñigo Flores Ituarte[1] · Jouni Partanen[1]

Received: 12 October 2017 / Accepted: 25 January 2018 / Published online: 10 March 2018

Abstract
The purpose of this research is to develop a computer-driven decision support system (DSS) to select optimal additive manufacturing (AM) machines for metal powder bed fusion (PBF) applications. The tool permits to evaluate productivity factors (i.e., cost and production time) for any given geometry. At the same time, the trade-off between feature resolution and productivity analysis is visualized and a sensitivity analysis is performed to evaluate future cost developments. This research encompasses a decision support system that includes a data structure and an algorithm which is coded in "MathWorks Matlab," considering cost structures for metal-based AM (i.e., machine cost, material cost, and labor cost). Results of this research demonstrate that feature resolution has a crucial effect on the total cost per part, but displays decreasing impacts for higher build volume rates. Based on assumptions of business consultancies, productivity can be increased, resulting in a potential decline of cost per part of up to 55% until 2025. Using this DSS tool, it is possible to evaluate the most optimal AM production systems by selecting between several input parameters. The algorithm allows industry practitioners to retrieve information and assist in decision-making processes, including cost per part, total cost comparison, and build time evaluations for typical commercial metal PBF systems.

Keywords Additive manufacturing · Powder bed fusion · Metals, decision support system · Feature resolution · Future cost evaluations

1 Introduction

Additive manufacturing (AM) and metal powder bed fusion (PBF) have become a serious competitor to conventional manufacturing processes [1]. Currently, the growth of this technology segment is supported by the fact that key original equipment manufacturers in the aerospace, automotive, and medical industries are integrating metal AM systems based on PBF technology to their manufacturing processes [2]. The technology offers many advantages, especially as it enables the manufacture of geometrically complex components in low- to mid-volume production [3]. Factors such as elimination of tooling reduce the up-front cost compared to conventional manufacturing methods [4]. To some extent, AM technologies have become enablers towards the digitized manufacturing as the technology is able to solve the "scale-scope dilemma." Hence, product variety and, therefore, mass customization can become feasible without cost penalties [5].

However, the implementation of AM into industry is challenged by cost and production speed parameters [6]. In practice, companies today have two options when evaluating AM for production applications. On the one hand, they aim at replacement or repair of components for their legacy systems. On the other hand, companies also want to benefit from newly designed AM parts for improved functional performance (e.g., part consolidation, topology optimization, decreased weight, etc.) [7]. Both applications encounter challenges with technology transfer decisions as the transition to AM has to be economically and technically substantiated.

Lately, attempts have been made to develop a DSS to support AM technology adaption. Literature has provided a holistic tool that can be used to select from multiple AM processes, machines, materials, and its final application type (e.g., rapid prototyping, rapid manufacturing, and rapid tooling) [8].

✉ Niklas Kretzschmar
niklas.kretzschmar@aalto.fi

[1] School of Engineering, Department of Mechanical Engineering, Production Technology, Aalto University, Puumiehenkuja 5, 02150 Espoo, Finland

Other studies have focused on developing web-based AM platforms, which allow to evaluate several technologies, collaborative manufacturers, and queuing of AM batches. However, the research on DSS for AM is highly fragmented with a need to link the existing body of knowledge to real and concrete industrial applications [9, 10].

In addition, metal PBF processes need to be validated to provide precise key performance indicators for technology transfer. The existing DSS designed for AM focuses on specialized plastic-based evaluation models [11], while metal-based PBF processes are rarely included. Due to the rapid development of PBF machines and the steps towards final industrial applications (e.g., four lasers up to 700 W, each operating simultaneously [12]), research needs to be conducted on productivity issues to assist their decision-making. The development of such DSS will be beneficial especially for companies that are considering to invest in metal-based AM machines.

Based on literature, the productivity of PBF has not been examined by implementing a quantitative model on a designed DSS focusing exclusively on metal PBF applications [13]. Therefore, this work can elucidate how companies and decision-makers can evaluate final production applications utilizing modern metal-based PBF machines from economical and technical perspectives. It presents the most relevant performance indicators to support the evaluation of PBF machines. Moreover, the existing trade-off between part quality and build volume rates and a predictive view on future events is outlined by investigating the impact of cost reductions for materials and machines.

2 Materials and methods

2.1 Classification scheme

The development of a DSS for metal-based AM components requires a classification scheme to describe the inner functional structure as well as interaction with the user. By applying the numerical computing software Matlab (version R2016b, Mathworks Natick, Massachusetts), a classification scheme is established which demands input parameters from the user. Figure 1 shows a schematic view of the DSS data structure. The first step is to upload the geometrical data of the part to be produced. For this reason, a STL (Standard Tessellation Language) file (i.e., an industry de facto standard file format for 3D representation which is native to most commercial AM systems) needs to be uploaded.

In the proposed system, the user can select or input relevant information. For predefined input values, the user is able to select from a series of common commercial machines and materials in a drop-down menu. In addition to this, different accuracy levels, production volumes, and densities of support structures can be selected. The DSS also accepts manual user parameters which allow more flexible evaluations and the possibility to forecast events such as a decrease in machine and material cost or an increase in production speed. Subsequently, the selected input parameters are examined in terms of feasibility regarding part dimensions and build sizes of selected AM machines. If the feasibility analysis is passed successfully, the algorithm proceeds to evaluate the PBF process economically and technically in terms of costs per part, cost type (divided into machine cost, material cost, and labor cost), production time (i.e., total production time function), number per batch, and ratio of support material.

2.2 Scheme for the input parameters

Figure 2 shows the graphical user interface of the DSS. As presented in the classification scheme, the user can either select predefined machines, materials, and accuracy levels (center left) or input the data manually (center right). Subsequently, the user can upload the part geometry by pressing the button *STL file import*. Imported data are then used to analyze part dimensions (i.e., x, y, and z dimensions of its bounding box) to calculate the number of parts fitting onto a specific build platform. The part volume is used to calculate process time and material cost, and the surface to improve build volume rate estimations. If the input data do not fulfill the machine criteria (e.g., part volume is too big for the selected machine), a failure code requests a change in the input data to start the simulation.

As an output, the DSS describes four process parameters (cost per part [€], the part process time [min], the number per batch [−], and the percentage of support [%]) and four figures (cost per part function, cost type, total time function, and a preview of the component). The current machine database supports the comparison between nine commercial AM machines. Out of these, eight are based on laser beam technology (Concept Laser "M2 cusing," Concept Laser "X LINE 1000 R," EOS "EOSINT M 280," EOS "EOSINT M 400," SLM Solutions "280 HL," SLM Solutions "500 HL," 3D System "ProX DMP 100," and the 3D System "ProX DMP 300") and one on electron beam technology (Arcam "Q10"). Each machine comprises specific maximum beam power levels (ranging from 50 to 3000 W), a wide machine price range between 226.000 € and 1.500.000 €, a varying number of processed materials, and inherent build volumes ranging from 800 cm^3 for the smallest and up to 120.000 cm^3 for the largest machine [14]. Regarding the material options, the DSS supports the selection of maraging steel, aluminum alloy, and titanium alloys (maraging steel DIN 1.2709, AlSi10Mg, and TiAl6V4 respectively). The implemented material prices amount to 89 € per kilogram for maraging steel DIN 1.2709 (density of 7.7 g/cm^3), 107 € per kg for aluminum alloys AlSi10Mg (density of 2.68 g/cm^3), and 400 € per kilogram for titanium alloys

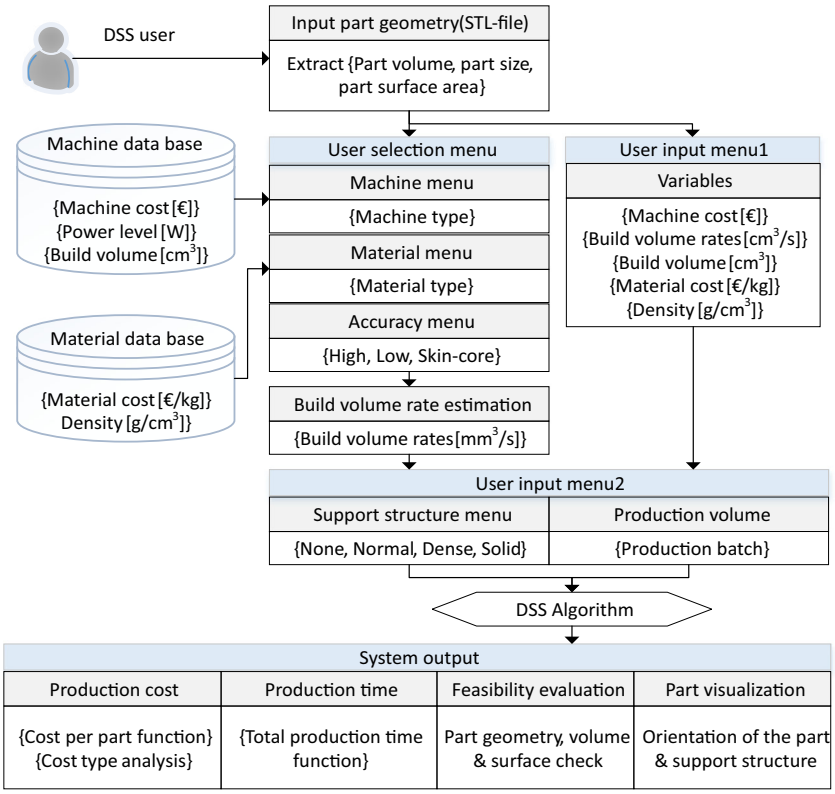

Fig. 1 AM classification scheme for predefined machines. Describes the workflow of the calculation tool including additional data to support the evaluations, from the input of a STL file to the output values and figure

TiAl6V4 (density of 4.45 g/cm^3), which are the underlying average values of the investigated price ranges [1, 15]. Furthermore, the material and machine databases can be reconfigured using the *manual input* to make projections for variables such as modified material costs, machine costs as well as build volume rates for each material.

The user can also select between three accuracy levels (i.e., *normal*, *high*, and *skin-core*) which have a direct impact on productivity. The normal accuracy mode enables higher build volume rates with a trade-off on part quality and geometrical features such as lower surface quality, feature resolution, and dimensional accuracy. In the normal accuracy mode, the DSS simulates the manufacturing process with beam powers operating at machines' full capacity. Therefore, by selecting this option, the user can maximize build volume rates at the cost of part quality and the benefit of lower production cost as well as high density levels of approximately 99.5%.

Conversely, high part quality has a negative impact on cost and build volume rates. In the high-accuracy mode, the DSS simulates the manufacturing process with a beam power

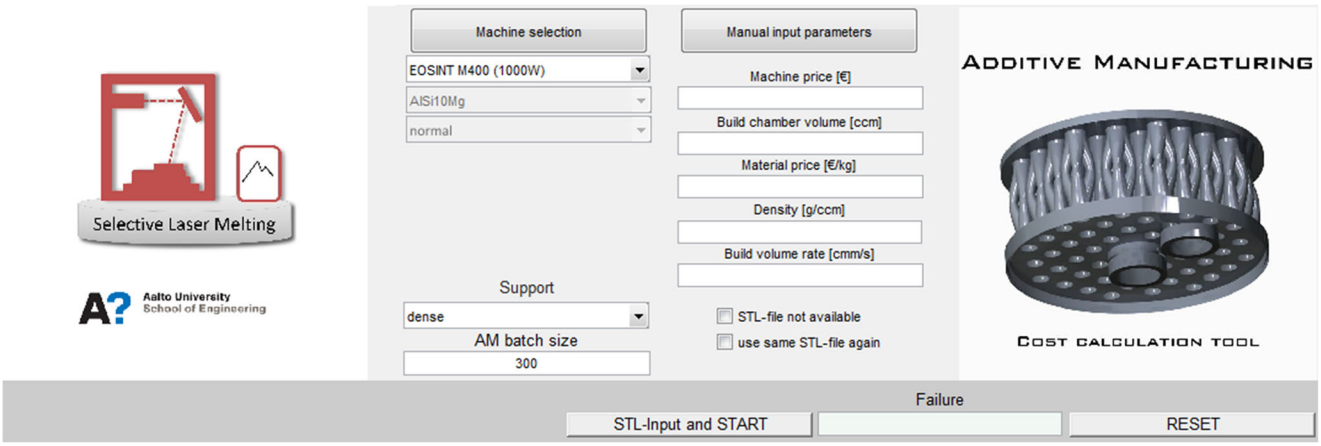

Fig. 2 Graphical user interface. The graphical user interface of the cost calculation tool consists of a predefined machine, material, and accuracy level selection (center left) as well as manual input parameters (center right). Additionally, information about the amount of support, the batch size, and the STL file needs to be provided by the user. This figure comprises all input fields the user is able to see before starting the calculations

operating at the lowest capacity of the machine (i.e., smaller beam diameters around 100 μm and layer thicknesses between 30 and 50 μm, depending on the selected machine technology). These sets of parameters are typically used to produce geometries with small geometrical features, resulting in an increase in part quality in terms of surface quality and feature resolution. In this study, all build volume rates are lowered by 40% taking the normal accuracy mode as a reference, when the high part quality mode is selected.

The third quality level is the skin-core methodology, which enables higher build volume rates and high surface quality characteristics at the same time. This method implies that the inner core area of parts is built with larger beam diameters, thicker layers, and higher beam powers (i.e., *normal*-quality characteristics) and the outer surface with *high*-quality characteristics. However, the skin-core technology requires overlaps between the skin and the core area, with a layer thickness ratio between inner and outer areas which cannot exceed 1:4. This means that by applying a skin layer thickness of 50 μm, the core layer thickness is limited to 200 μm. Suitable porosity levels only occur when providing an overlap area between inner and outer layer thicknesses. For a skin-core ratio of 1:2, the overlap area is typically 0.5 mm, whereas an overlap of 0.75 mm is necessary for a skin-core ratio of 1:4. Furthermore, the width of the skin area can be expected to amount to approximately 1 mm [16]. Out of the nine machines, this specific mode can only be selected for the machine EOSINT M 280 [17], for all other machines this mode is blocked.

2.3 Theory and calculations

2.3.1 Build volume rates and productivity—criteria for part quality

Build volume rates $\dot{V}\left[\frac{mm^3}{s}\right]$ are described by the material volume being created from the metal powder over time. They represent the main productivity factor and have a major impact on lowering the AM production cost by means of time savings. Equation (1) describes the theoretical build volume that can be calculated by multiplying the layer thickness D_S (μm), the scan speed v_{scan} $[\frac{mm}{s}]$ and the scan line spacing (distance between parallel laser tracks) Δy_s (μm).

$$\dot{V} = D_S * v_{\text{scan}} * \Delta y_s \tag{1}$$

Moreover, in many cases, the scan line spacing can be formulated as [18]:

$$\Delta y_s = 0.7 * d_s \tag{2}$$

where d_s denotes the focus diameter (mm) of the energy source (i.e., laser or electron beam in PBF systems) and the constant factor of 0.7 denotes the side shift of the laser in the melt pool. However, the scan line spacing parameter can vary significantly dependent on machine equipment, material, power levels, layer thicknesses, etc. [19]. The v_{scan} parameter is dependent on the intensity I $[\frac{W}{mm^2}]$ and the required layer thickness D_S. If intensity is high and the required layer thickness is low, higher scan speed can be achieved, whereas low intensities and large layer thicknesses lead to lower scan speeds. Furthermore, intensity represents the quotient of laser power P [W] and area A $[mm^2]$. The affected area in the powder bed can be calculated by means of Eq. (3):

$$A = \frac{1}{4} * d_s^2 * \pi \tag{3}$$

Predefined laser power directly affects scanning speeds as well as beam diameters d_s (mm), whereas part quality varies by changing scan speeds and laser power. A main parameter when estimating AM system productivity is the machine build volume rate. This value is the result of the interactions between several physical and machine process parameters, such as beam power, hatch size, scanning speed, scan line spacing, layer thickness, and material properties. An estimation of build volume rates from literature was executed [16, 20–26], necessary for the implementation into the DSS.

Figure 3 shows that TiAl6V4 reaches the highest build volume rates including a coefficient of determination (COD) of 63%, followed by AlSi10Mg (COD 93%), and maraging steel DIN 1.2709 (COD 81%). Parameters such as the degree of absorption, particle size, and distribution, as well as materials' melting points, have an effect on deviating build volume rates. However, this figure outlines results for porosity levels below 2% only, which displays fully melted parts, guaranteeing sufficient mechanical properties for most engineering applications.

Feature resolution is one of the main characteristics in the production of metal-based AM parts. In this regard, the smaller the beam diameter and layer thickness, the higher the feature resolution of the part being produced. To ensure suitable quality, parts with high-feature resolution need to be processed with lower laser beam powers and scan line spacing [27]. Consequently, the build volume rate, which was described in Eq. (1), decreases and causes rising costs due to a higher manufacturing time per part.

2.3.2 Underlying algorithm

Referring to cost models for plastic-based laser sintering [28] and metal-based powder bed fusion [29], this approach can be seen as an adaptation and practical

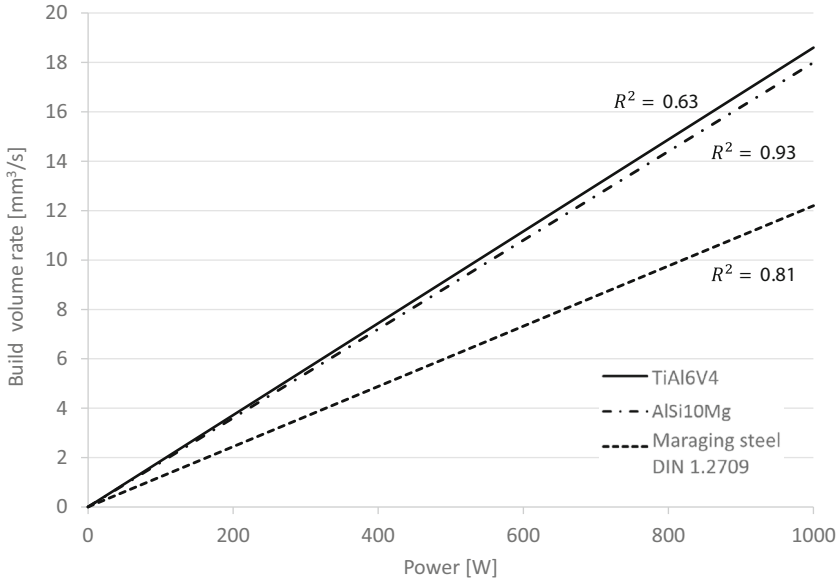

Fig. 3 Build volume rates for maraging steel DIN 1.2709, AlSi10Mg, and TiAl6V4 for porosity levels under 2%. Each line represents a specific build volume rate for a certain power level. Higher power levels lead to a linear increase of the build volume rate

application to already existing models. Figure 4 displays the developed algorithm structured into three different cost types: machine costs c_{eom}, labor costs c_{eow}, and material costs c_{mat}. Each arrow transfers the output of one formula as an input to the consecutive one, each dashed line describes a connection between two different kinds of cost types. Adding up calculated cost types leads to the cost of the build c_{ob} [€] and finally to the cost of the part c_{op} [€] by dividing the number of the total cost of the build through the part number p_n [−]. All symbols in the algorithm are described in Table 1.

2.3.3 Machine costs

The surface area ratio r is described by the outer volume V_s, which is evaluated by multiplying the surface area S and the width of the skin area s_t. To calculate the ratio between skin and core areas, the outer volume has to be divided by the part volume p_v. This ratio is based on the selected accuracy level and has an effect on the average build volume rate v_m, influencing the build time significantly. High accuracy is described by a ratio $r = 1$, normal accuracy by a ratio $r = 0$. Skin-core accuracy has a range

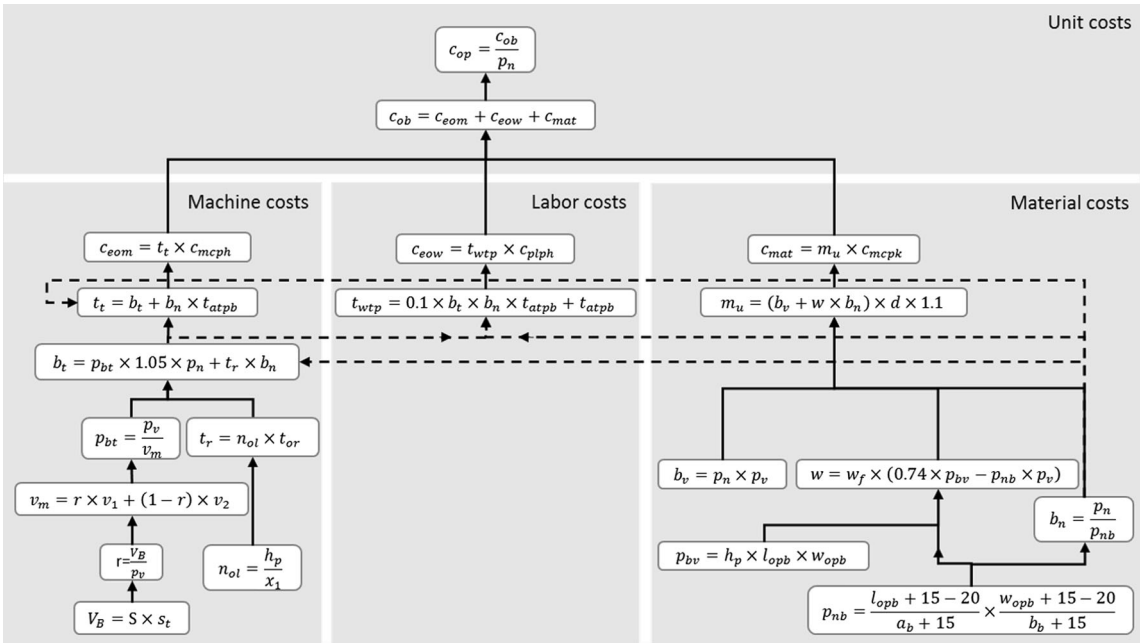

Fig. 4 Underlying DSS algorithm. This figure shows the most important formulas, their connection to each other, and to which category they belong to regarding the DSS algorithm

of $0 < r < 1$, which is dependent on the extent of surface area of the part.

If $r = 0$, it means that the value v_1 will not influence the average speed v_m. However, high accuracy with a ratio of 1 leads to an average speed, exclusively containing v_1.

$$v_m = r \times v_1 + (1-r) \times v_2 \tag{4}$$

where v_1 represents the high-quality build volume rate and v_2 the normal-quality build volume rate.

The build time b_t is derived from [7], it consists of the summation of three major time factors, which are represented by the scan time T_S, the recoating time T_r, and the delay time T_e. When transferring this formula to the cost model presented in Fig. 4, the delay time amounts to 5% and is added to the scan time. This additional factor is added due to process inequalities.

$$b_t = p_{bt} \times 1.05 \times p_n + t_r \times b_n \tag{5}$$

where b_t represents the build time, p_{bt} represents the part build time, p_n represents the part number, t_r represents the recoating time, and b_n represents the number of batches.

Recoating time is calculated over the number of layers n_{ol}, which slices the part height h_p (dependent on the part orientation) into constant layer thicknesses x_1. The layer thickness parameter is set at 50 μm for all parts and is not dependent on the accuracy level. Moreover, the recoating time includes a constant recoating time factor of 4.5 s per layer. Consequently, the recoating time factor has to be multiplied with the number of layers.

Expenses on machine c_{eom} are described by the following mathematical relationship: the total time t_t is calculated by taking the build time b_t and adding extra times per batch t_{atpb} multiplied with the batch number b_n. These additional time factors per batch are assumed to stay on a constant level for all printing processes (for each batch) in this study. According to [29], a preparation time of $T_{\mathrm{prep}} = 0.25$ h, build job time of $T_{\mathrm{Buildjob}} = 0.25$ h, setup time of $T_{\mathrm{Setup}} = 0.75$ h, removal time of $T_{\mathrm{Removal}} = 0.5$ h, and post-processing time of $T_{\mathrm{Postp}} = 0.1$ h are taken into account. This results in a potential total labor time for each batch of $t_{\mathrm{atpb}} = 1.85$ h/batch, which represents a rather low additional time factor per batch. In this study, t_{atpb} amounts 3 h/batch, including heating and cooling times as well as longer removal times of 35 min [30].

To estimate expenses on machine c_{eom}, the total time t_t is multiplied with the parameter machine cost per hour c_{mcph}.

Machine costs per hour c_{mcph} are calculated by assuming that the laser beam and electron beam based machines in this study total 120 h/week in use. This represents a 24-h usage during the 5 working days of a week. Furthermore, a maximum machine usage of 51 weeks per year totals 6120 h/year of possible machine utilization. Considering that 1 year consists of 8736 h, the outlined machine utilization of 6120 h/year t_{mh} results in an utilization rate of 70%, which is assuming that the production is also running during nights and delays for reparations are obsolete. However, leading manufacturing companies produce their goods on weekends as well; hence, a utilization rate of 70% seems to be appropriate for series production of AM components.

Table 1 List of symbols referring to the DSS algorithm. It depicts the symbols, units, and meanings applied in the DSS algorithm in Fig. 4

Symbol	Unit	Meaning
a_b	mm	Length of the part
b_b	mm	Width of the part
b_n	–	Batch number
b_t	s	Build time
h_p	mm	Height of the part
V_B	m^3	Volume of the build
V_S	mm^3	Outer volume
c_{hc}	€	Hardware cost
c_{eom}	€	Expenses on machine
c_{eow}	€	Expenses on worker
c_{mat}	€	Material costs
c_{mc}	€	Maintenance cost
c_{mcph}	€	Machine cost per hour
c_{op}	€	Cost of part
c_{pc}	€	Purchase depreciation
c_{plph}	€	Production labor cost per hour
c_{sc}	€	Software cost
l_{opb}	mm	Length of the powder bed
m_u	mm^3	Material used
n_{ol}	–	Number of layers
p_{bt}	s	Part build time
p_n	–	Part number
p_{nb}	–	Part number per batch
p_v	mm^3	Part volume
t_{atpb}	s	Additional time per batch
t_{mh}	h	Machine utilization
t_r	s	Total recoating time
t_{or}	s	Recoating time per layer
t_t	s	Total time
t_{wtp}	h	Workers time paid
v_1	$\frac{mm^3}{s}$	High-quality build volume rate
v_2	$\frac{mm^3}{s}$	Normal-quality build volume rate
v_m	$\frac{mm^3}{s}$	Average build volume rate
w_f	–	Waste factor
w_{opb}	mm	Width of the powder bed
r	–	Skin-core ratio
S	mm^2	Surface area
s_t	mm	Accurate surface thickness
w	mm^3	Waste material
ρ	$\frac{kg}{m^3}$	Density

Purchase depreciation c_{pc} is calculated using 8 years for production machines and 5 years for software. Hence, the purchase price has to be divided by 8 and the software purchase price by 5. This depreciation varies from machine to machine and contains a significant impact on the total cost per part value. Maintenance, software, and hardware costs were transferred from a previous study [31] and are expected to be of constant value. Therefore, according to a depreciation time of 5 years for each of them, 21,750 € has to be spent on maintenance each year c_{mc}, 1450 €/year for software c_{sc}, and 870 €/year for hardware c_{hc}. To estimate machine costs per hour, the following formula is implemented into the calculation tool.

$$c_{mcph} = c_{pc} + c_{mc} + c_{sc} + c_{hctmh} \tag{6}$$

where c_{mcph} denotes the machine cost per hour, c_{pc} denotes the purchase depreciation, c_{mc} denotes the maintenance cost per year, c_{sc} denotes the software cost per year, c_{hc} denotes the hardware cost per year, and t_{mh} denotes the amount of machine hours.

2.3.4 Material costs

Batch sizes describe the number of products being manufactured during one set, varying for each bounding box of a machine. Depending on the planned approach to place parts into the powder bed, a specific number of parts p_{nb} can be calculated through [7]:

$$p_{nb} = \left(l_{opb} + 15{-}20a_b + 15\right) \times \left(w_{opb} + 15{-}20b_b + 15\right) \tag{7}$$

in which l_{opb} represents the horizontal direction of the powder bed and w_{opb} represents the vertical direction of the powder bed. Fifteen millimeters is used for the gaps between the bounding boxes in x and y—direction and part length are described by a_b, and the width of the part is described by b_b.

The filled powder bed volume p_{bv} depends on the height of parts h_p which is multiplied by the length of the powder bed l_{opb} and the width of the powder bed w_{opb}. Consequently, a filled-up build chamber is calculated without inserted parts.

Unused powder (waste material w) of the filled powder bed can be recycled with an efficiency between 95 and 98% [32]. This factor is called waste factor w_f in this study. Therefore, the volume of the filled powder bed is calculated by assuming a hexagonal closest particle packing ratio of 0.74 (74%). This ratio is multiplied with the length and height of the specific powder bed and its fill-up height depends on the part height. Subsequently, the number of produced parts multiplied by the volume of each part is deducted from the theoretical filled powder bed. By including a waste factor of 0.02, the calculations finally lead to the wasted material w.

$$w = w_f \times \left(0.74 \times p_{bv}{-}p_{bn} \times p_v\right) \tag{8}$$

where w_f denotes the waste factor, p_{bv} denotes the filled powder bed volume, p_{bn} denotes the batch size estimator, and p_v denotes the part volume.

The build volume b_v and the number of batches b_n are calculated by multiplying the part number p_n and the part volume p_v. To evaluate b_n, the part number p_n is divided by the number of parts in each bed p_{nb}, which is defined by the batch size estimator.

The total volume (material used m_u), consisting of build volume b_v and waste w, is evaluated over the density of each material. The build volume as well as the additional support value are calculated by an approximation of the STL file.

$$m_B = d \times p_v \tag{9}$$

where m_B outlines the part mass, d outlines the density, and p_v outlines the volume. Support structures have to be established for structural stability during the printing process. This issue is addressed by adding a constant factor of 10% (α) extra to the part volume in the case of manual data input (STL file not available). To estimate the amount of support more accurately (STL file available), uploaded models are oriented into varying poses of 5° increments for each coordinate axis. For each orientation, all triangles with downwards-pointing normal vectors (i.e., 3D angle deviating less than the threshold angle of 45° from the downward vector) are located. Consequently, the irregular prism volumes are calculated from each triangle to the build platform and by summing up these subvolumes, the total amount of support is evaluated. The orientation, which produces the smallest support volume, is returned as the value for the "solid" support strategy. To approximate more common rod-type supports, users also have an option to choose between "normal" and "dense" support strategies; by selecting one of these, the returned support volume value is scaled by 0.2 and 0.5, respectively.

The estimated material m_u being used has to be multiplied with the cost per each kilogram c_{mcpk}, which differs significantly depending on the type of material being used. Maraging steel DIN 1.2709, AlSi10Mg, and TiAl6V4 can be selected as input material in the AM tool. As a result, the user receives the material cost value c_{mat}.

2.3.5 Labor costs

For the workers' paid time t_{wtp}, the employee is not expected to work full time for the manufacture of AM parts. In detail, the employee is paid for the setup time, the reprocessing time of each batch, and a monitoring time of 10% during the

printing process. This factor has to be multiplied with the build time b_t. Moreover, the additional time per batch t_{atpb} depending on the number of batches is added. The expenses on worker c_{eow} are calculated as the product of the workers' paid time t_{wtp} and the production labor cost per hour c_{plph}. It varies depending on the country (Western European salary assumed in this study) and the required qualifications of the employee. In summary, expenses on worker c_{eow}, expenses on machine c_{eom}, and material cost lead to the total cost of the build c_{ob}.

2.4 Experimental analysis assisted by the DSS

An example geometry is adopted to run experiments with the DSS. A timing pulley with inner structures as represented in Fig. 5 is selected to model and examine different manufacturing scenarios. Distances between each timing pulley are determined by the batch size estimator and do not change according to the size of the part after its orientation.

As input parameters, the geometry is scaled from 7.5 to 135 mm in height, assuming 10 different part heights (part 1 to part 10). Moreover, a constant production volume of 300 parts is tested. The implemented machine during the test is an EOSINT M 400 with a base price of 1,250,000 € [33] and a build platform of 400 × 400 × 400 mm. The investigated materials comprise maraging steel DIN 1.2709 (material price 89 €/kg), aluminum alloy AlSi10Mg (material price 107 €/kg), and titanium alloy TiAl6V4 (material price 400 €/kg); the selected support structure is "dense." Table 2 describes a list of parts with scaled heights (z), resulting in higher x and y dimensions as well as in volume increases.

Cost estimations including all 10 parts for different materials and accuracy levels are conducted. Additionally, price quotes for the same components, materials (except for maraging steel DIN 1.2709, not selectable), and production volume are presented to discuss results.

To analyze the influence of the build volume rate on production costs, part 5 with a height of 60 mm is selected and evaluated for varying build volume rates and materials for the "normal" accuracy level.

Finally, to conduct a sensitivity analysis of the DSS and to evaluate future implications for material and machine cost reduction, this study refers to the projections of a business consultancy [1]. According to their projections, cost reductions for materials as well as machines are expected to decline significantly in the coming years, ranging from 25 to 45%. To test possible future scenarios and the impact of these estimations, material and machine costs are lowered by 20, 40, and 60% for projections until 2025. The material maraging steel DIN 1.2709, "normal" accuracy, and "dense" support structures are selected.

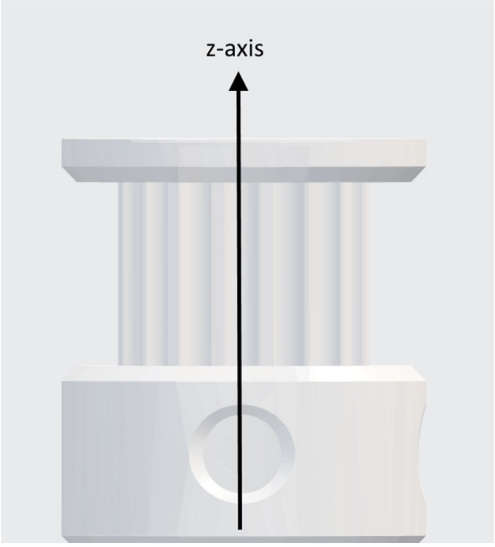

Fig. 5 Scaled timing pulley. This example geometry is scaled proportionally in height (z-axis) to analyze the DSS algorithm

3 Results and discussion

To assist in the decision-making process, the DSS delivers four key performance indicators and three different functions (Fig. 6), which are crucial when evaluating AM application suitability. This set of outputs comprises a cost function, which is dependent on the number of parts, a cost type analysis, a preview of the part consisting of the orientations and the support structure (side and front view, vertical thick lines represent the support structure) and a total time function.

As key performance indicators, a cost per part value for the selected production volume (€), the part process time (min), the producible number per batch (−), and a support value (%) are illustrated in Fig. 6. These values and graphs allow economic and AM specific conclusions for any metal component to be produced using AM technologies.

Table 3 shows cost estimations for the mentioned input parameters. When the parts are scaled proportionally (z-height as the reference axis), a lower amount of parts fits into one production batch, leading to a drop from 288 for part 1 to 5 for part 10. The support value varies between 8.07 and 12.66% and costs increase significantly for evaluated components, ranging from 1.23 € for part 1 produced out of AlSi10Mg to 11,414 € for part 10 selecting TiAl6V4 as the manufacturing

Table 2 Parameters of the scaled timing pulley. The component is scaled up from 7.5 to 135 mm in height, showing modified dimensions and volumes

Part no.	x (mm)	y (mm)	z (mm)	V (cm^3)
1	6.73	6.72	7.5	0.15
5	53.81	53.8	60	78.71
10	121.06	121.04	135	896.52

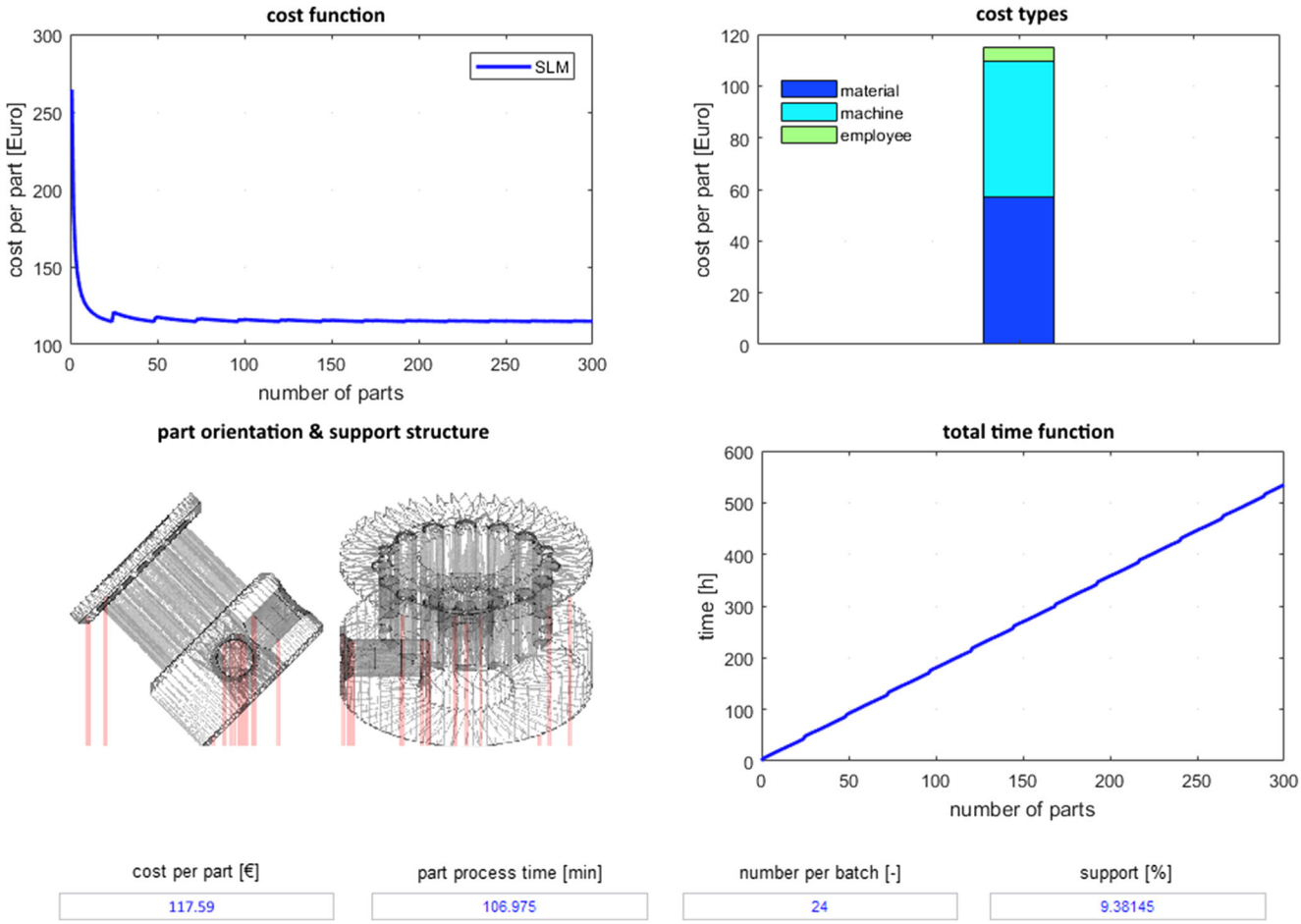

Fig. 6 Graphical interface of DSS outputs including key performance indicators and figures (timing pulley part 5). Several functions and a screenshot of the part are shown at the top of this figure, whereas four key performance indicators are displayed below them

material. Estimated costs represent in most cases lower values than the online price quotes, especially for the smaller parts 1–5. For larger components (parts 8–10), the differences between estimated costs and price quotes from the AM service provider decrease, in the case of TiAl6V4, costs exceed the prices.

Table 3 Cost estimations for the scaled timing pulley using the normal-accuracy (NA) and the high-accuracy (HA) mode, price quotes [34] applying same input data as well as batch sizes and support values for 300 parts being printed and dense support structures being selected

Part no.	z (mm)	Batch size (−)	Support value (%)	AlSi10Mg			Maraging steel DIN 1.2709		SS316L	TiAl6V4		
				Cost NA (€)	Cost HA (€)	Price quote (€)	Cost NA (€)	Cost HA (€)	Price quote (€)	Cost NA (€)	Cost HA (€)	Price quote (€)
1	7.5	288	9.39	1.23	1.30	n.d.	1.37	1.47	n.d.	1.59	1.66	n.d.
2	15	157	9.38	2.42	2.93	24.9	3.39	4.17	37.36	4.86	5.37	48.56
3	30	68	9.29	14.02	18.13	74.52	21.20	27.47	111.78	34.22	38.33	145.32
4	45	37	9.29	46.61	60.47	185.67	69.82	90.96	278.5	124.62	138.49	362.05
5	60	24	9.38	117.59	150.43	384.58	170.14	220.26	576.87	332.96	365.85	749.93
6	75	16	8.07	244.43	308.57	696.76	343.67	441.56	1045.1	715.39	779.63	1358.7
7	90	12	11.64	549.61	660.43	1151.6	698.07	867.22	1727.4	1722.9	1833.9	2245.6
8	105	9	11.57	1011.9	1187.9	1775.9	1223.4	1420.0	2663.9	3264.3	3440.6	3463.1
9	120	7	9.38	1542.2	1804.9	2589.5	1851.3	2252.3	3884.2	5210.1	5266.2	5049.5
10	135	5	12.66	3343.1	3717.2	3626.6	3594.2	4165.1	5439.8	11,414	11,789	7071.8

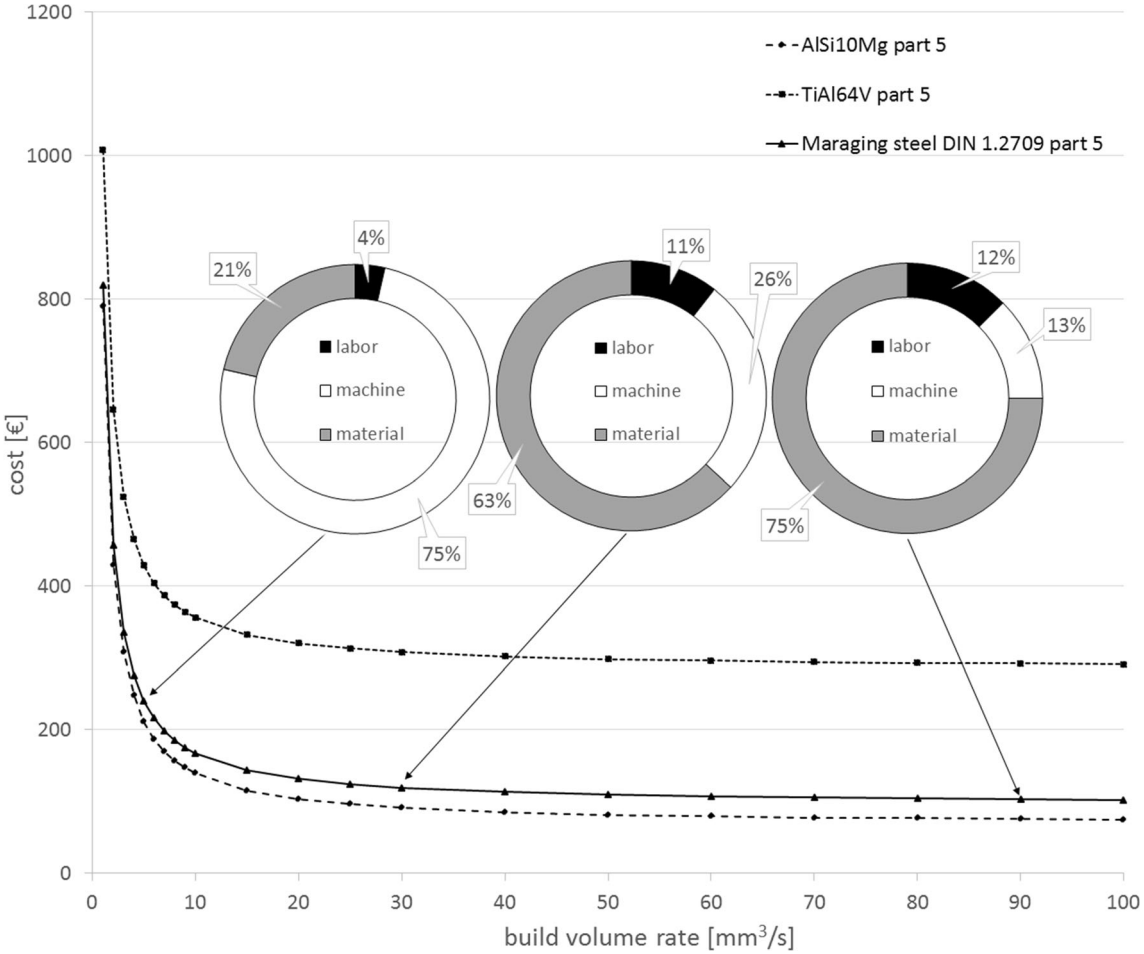

Fig. 7 Cost development for increased build volume rates of part 5. The effect of increased build volume rates on production costs is demonstrated for a timing pulley, which is produced additively out of three different materials. Each circle describes the cost structure regarding a specific build volume rate for the usage of maraging steel DIN 1.2709

Presented price quotes cannot be compared directly with the calculated costs from the DSS, but represent a benchmark if profits and additional parameters such as energy consumption and rental costs would be included in the DSS.

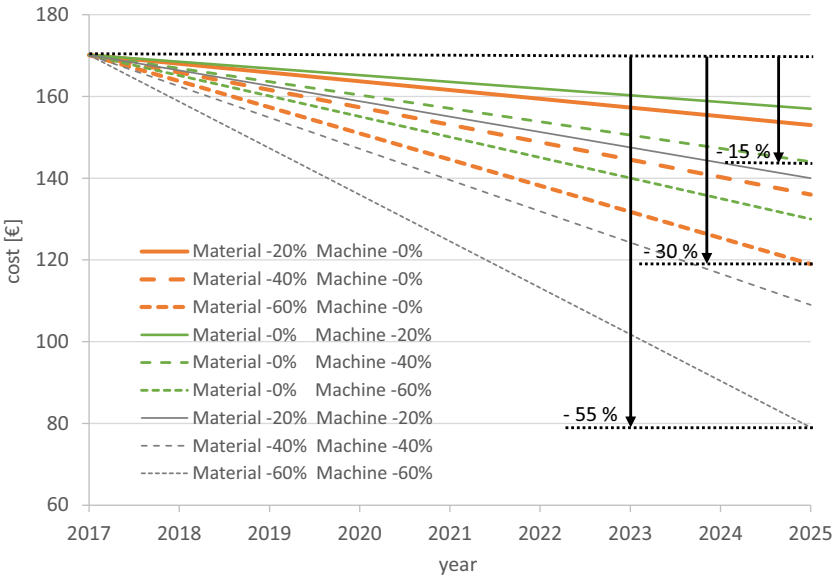

Fig. 8 Future cost estimations for part 5 for maraging steel DIN 1.2709. This figure provides future cost estimations regarding several scenarios, which arise from a decline in material and/or machine costs. Each vertical arrow shows the total cost decrease for three selected scenarios

Additionally, the lack of knowledge regarding company-specific aspects such as their pricing strategy, existent AM PBF machines, material procurement prices, and special build strategies to optimize the production workflow does not allow direct quantitative comparisons. Considering mentioned aspects, cost results appear meaningful, while errors in the DSS can arise from several factors such as standardized additional batch time parameters, non-machine type-related build volume rates (generalized approach according to their beam power), and unrealistic literature-based material as well as machine prices.

Figure 7 analyzes quantitatively the economical trade-off between part quality and build volume rates, taking part 5 as a reference. The trade-off can be described as a non-linear development of increased build volume rates ranging from 0 to 100 mm^3/s. The results indicate that significant cost decreases can be achieved between 0 and 10 mm^3/s, moderate cost decreases between 10 and 20 mm^3/s, and insignificant cost decreases between 20 and 100 mm^3/s for all the selected materials. Using a maximum build volume rate of 100 mm^3/s leads to cost values of 50 €/part for AlSi10Mg, 80 €/part for maraging steel DIN 1.2709, and 180 €/part for TiAl6V4.

After a build volume rate of 40 mm^3/s is achieved, the effect on the reduction of production cost is decreased drastically. In this regard, intrinsic machine parameters, such as the recoating time and the machine set up time, are independent from the other variables such as laser power, scan spacing, and layer thickness. Hence, a reduction of production cost derived from the increase in build volume rate in PBF machines is unsustainable. In fact, titanium alloys have the lowest saving potential for build volume rates from 20 to 100 mm^3/s due to high material prices. The pie chart allows a more detailed view at the evolution of cost structures as a function of the build volume rate. Using maraging steel DIN 1.2709 as the input material, the machine costs decrease for increased build volume rates of 5, 30, to 90 mm^3/s, whereas the percentages of material and labor costs increase permanently. Cost differences between materials can be traced back to varying material prices and densities of parts but not to deviating labor and machine costs, which stay constant for each material. The most critical factor for AM adaption is material cost and the effect of increasing build volume rates which have no strong impact on the production cost.

Figure 8 shows the impact of future cost development in time (x-axis) for metal-based AM parts in relation to the example geometry and its production cost per part (y-axis). When material and machine costs are decreased by 60% each, the total costs per part can be lowered by 55%, while a 30% decrease in total costs is observed when material cost is decreased by 60%.

Due to an already significant and growing number of metal powder providers and a more severe competition among them, prices are expected to decline [1]. However, similar competitive circumstances are absent in the market segment for high-end metal-based PBF machines with powers over 1000 W. On the one hand, there are two different processes (laser beam and electron beam based) that fit for different purposes. On the other hand, only few companies are able to produce high-end AM metal machines for high-quality component production. Assuming that the material costs will decrease by 60%, the machine cost will stay on the same level. Further improvements in the production speeds can be achieved, resulting in a cost-saving potential of 40 to 45% by 2025 for AM metal part production in total.

The sensitivity analysis indicates that a drop in material prices has a more significant impact on modern metal-based AM machines than changes in the machine prices. The future price developments outlined can be understood as generic trends, because the cost of production per voxel (mm^3) appears constant for a particular material.

4 Conclusion

Based on the gained experimental results, we can conclude that to achieve competitiveness of metal PBF machines in production environments, the machine build volume rate has to exceed 20 mm^3/s for this specific machine. When reaching or exceeding this value, potential cost savings are mostly dependent on the material cost.

In addition, the part size has no direct effect on the cost-saving potential. All parts (1 to 10) show a potential cost-saving factor of approximately 90% depending on build volume rates varying from 1 to 100 mm^3/s. These results were obtained by examining costs for all parts (1–10). In this regard, feature resolution becomes a substantial cost driver in metal-based AM (especially for normal build volume rates, 1 to 5 mm^3/s in this case), which should be avoided whenever it is possible to make PBF production applications viable.

To decrease future total part costs, material prices need to decrease and a higher degree of automation should be achieved. The purchasing costs of AM machines constitute no decisive factor in modern series AM production, if high utilization rates can be achieved. For high-cost materials (e.g., TiAl6V4), the importance of decreasing material prices is even more significant, while for low-cost materials (e.g., AlSi10Mg), the influence of machine prices dominates.

Acknowledgements The authors wish to thank Eero Huotilainen for supporting us in the use of the software Matlab.

Compliance with ethical standards

Conflict of interest The authors declare that they have no conflict of interest.

References

1. Langefeld B, Schäff C, Beenker H, Balzer C (2016) Additive manufacturing—next generation. In: Rol. Berger Strateg. Consult. https://www.rolandberger.com/publications/publication_pdf/roland_berger_additive_manufacturing_next_generation_amnx_study_20160412.pdf. Accessed 12 Jan 2018
2. Bradley B (2016) Metal AM part production. In: Wohlers Report 2016. pp 183–194
3. Flores Ituarte I, Partanen J, Khajavi SH (2016) Challenges to implementing additive manufacturing in globalised production environments. Int J Collab Enterp 5(3/4):232–247. https://doi.org/10.1504/IJCENT.2016.10003181
4. Baumers M, Dickens P, Tuck C, Hague R (2016) The cost of additive manufacturing: machine productivity, economies of scale and technology-push. Technol Forecast Soc Change 102:193–201. https://doi.org/10.1016/j.techfore.2015.02.015
5. Petrick IJ, Simpson TW (2013) 3D printing disrupts manufacturing: how economies of one create new rules of competition. Res Manag 56(6):12–16. https://doi.org/10.5437/08956308X5606193
6. Lindemann C, Jahnke U, Moi M, Koch R (2012) Analyzing product lifecycle costs for a better understanding of cost drivers in additive manufacturing. Int Solid Free Fabr Symp 23:177–188. https://doi.org/10.1007/s13398-014-0173-7.2
7. Gibson I, Rosen DW, Stucker B (2010) Additive manufacturing technologies: rapid prototyping to direct digital manufacturing. Springer. p 1–459. https://doi.org/10.1007/978-1-4419-1120-9
8. Byun HS, Lee KH (2005) A decision support system for the selection of a rapid prototyping process using the modified TOPSIS method. Int J Adv Manuf Technol 26(11-12):1338–1347. https://doi.org/10.1007/s00170-004-2099-2
9. Lan H, Ding Y, Hong J et al (2004) A web-based manufacturing service system for rapid product development. Comput Ind 54(1):51–67. https://doi.org/10.1016/j.compind.2003.07.006
10. Lan H (2009) Web-based rapid prototyping and manufacturing systems: a review. Comput Ind 60(9):643–656. https://doi.org/10.1016/j.compind.2009.05.003
11. Ghazy MM (2012) Development of an additive manufacturing decision support system (AMDSS). https://theses.ncl.ac.uk/dspace/bitstream/10443/1692/1/Ghazy 12.pdf. Accessed 12 Jan 2018
12. SLM Solutions (2017) Selective laser melting machine SLM 500. https://slm-solutions.de/produkte/maschinen/selective-laser-melting-maschine-slm-500. Accessed 12 Jan 2018
13. Costabile G, Fera M, Fruggiero F et al (2016) Cost models of additive manufacturing: a literature review. Int J Ind Eng Comput 8:263–282. https://doi.org/10.5267/j.ijiec.2016.9.001
14. Verlag moderne Industrie GmbH (2011) Marktübersicht "Generative Fertigungsanlagen". In: Das Fachmagazin für die Met. http://docplayer.org/7768781-Marktuebersicht-generative-fertigungsanlagen-vollstaendige-version-der-marktuebersicht-aus-fertigung-10-11-11-ausgabe-oktober-november-2011.html. Accessed 29 Dec 2017
15. EOS GmbH (2014) Material pricing EOS materials plastics EOS materials metals applicable materials for EOS M 290. https://www.cmu.edu/ices/advanced-manufacturing-laboratory/eos-materials-price-list_06-19-14.pdf. Accessed 14 Aug 2016
16. Schuh G, Behr M, Brecher C, et al (2012) Integrative production technology for high-wage countries: Individualised production. Springer. p 77–239. https://doi.org/10.1007/978-3-642-21067-9
17. Lippert RB, Lachmayer R (2018) Industrializing additive manufacturing—proceedings of additive manufacturing in products and applications—AMPA2017. Springer. p 14-23. https://doi.org/10.1007/978-3-319-66866-6
18. Buchbinder D, Schleifenbaum H, Heidrich S et al (2011) High power selective laser melting (HP SLM) of aluminum parts. Phys Procedia 12:271–278. https://doi.org/10.1016/j.phpro.2011.03.035
19. Kamath C, Gallegos GF, Sisto A (2013) Density of additively-manufactured, 316L SS parts using laser powder-bed fusion at powers up to 400W. Univ North Texas Libr Digit Libr. p 1-19. https://doi.org/10.2172/1116929
20. Yasa E, Craeghs T, Badrossamay M, Kruth J-P (2009) Rapid manufacturing research at the Catholic University of Leuven. RapidTech 2009, PP 1–10
21. EOS GmbH (2011) Material data sheet EOS maraging steel MS1. http://ip-saas-eos-cms.s3.amazonaws.com/public/1af123af9a636e61/042696652ecc69142c8518dc772dc113/EOS_MaragingSteel_MS1_en.pdf. Accessed 12 Jan 2018
22. Krishnan M, Atzeni E, Canali R, Calignano F, Manfredi D, Ambrosio EP, Iuliano L (2014) On the effect of process parameters on properties of AlSi10Mg parts produced by DMLS. Rapid Prototyp J 20(6):449–458. https://doi.org/10.1108/RPJ-03-2013-0028
23. EOS GmbH (2014) Material data sheet for EOS titanium Ti64 for EOSINT M 270 systems. https://cdn0.scrvt.com/eos/bfa4cd276d352f1f/f6008c2914f3/EOS-Titanium-Ti64ELI.pdf. Accessed 12 Jan 2018
24. Rosenthal I, Stern A, Frage N (2014) Microstructure and mechanical properties of AlSi10Mg parts produced by the laser beam additive manufacturing (AM) technology. Metallogr Microstruct Anal 3(6):448–453. https://doi.org/10.1007/s13632-014-0168-y
25. Ilt F, Laser C (2012) Lasered aluminium could supplant machined car parts. https://www.concept-laser.de/fileadmin/user_upload/1211_X_line_ETMM_12-2012.pdf. Accessed 12 Jan 2018
26. Karg M, Hentschel O, Ahuja B, et al (2016) Comparison of process characteristics and resulting microstructures of maraging steel 1.2709 in additive manufacturing via laser metal deposition and laser beam melting in powder bed. 6th Int Conf Addit Technol Nürnberg, Ger
27. Frazier WE (2014) Metal additive manufacturing: a review. J Mater Eng Perform 23(6):1917–1928. https://doi.org/10.1007/s11665-014-0958-z
28. Atzeni E, Salmi A (2012) Economics of additive manufacturing for end-usable metal parts. Int J Adv Manuf Technol 62(9-12):1147–1155. https://doi.org/10.1007/s00170-011-3878-1
29. Rickenbacher L, Spierings A, Wegener K (2013) An integrated cost-model for selective laser melting (SLM). Rapid Prototyp J 19(3):208–214. https://doi.org/10.1108/13552541311312201
30. EOS GmbH (2014) EOS–corporate presentation. http://www.efestolab.com/doc.php?n=15. Accessed 20 Jan 2018
31. Ruffo M, Hague R (2007) Cost estimation for rapid manufacturing—simultaneous production of mixed components using laser sintering. Proc Inst Mech Eng Part B J Eng Manuf 221(11):1585–1591. https://doi.org/10.1243/09544054JEM894
32. Berman B (2012) 3-D printing: the new industrial revolution. Bus Horiz 55(2):155–162. https://doi.org/10.1016/j.bushor.2011.11.003
33. Wohlers T (2016) Wohlers report 2016. 3D printing and additive manufacturing state of the industry: System specifications. Wohlers associates. p 305-322.
34. AM service provider Materialise OnSite. https://onsite.materialise.com/. Accessed 20 Jan 2018